On-Chip Cascaded Bandpass Filter and Wavelength Router Using an Intelligent Algorithm

Hongyi Yuan, Lifeng Ma, Zhe Yuan, Shuai Feng, Jing Li, Xiaoyong Hu, and Cuicui Lu

***Abstract*—Cascaded nanophotonic devices play a vital role in all-optical connection, all-optical computation and all-optical network. However, there is almost no effective method for the direct design of on-chip cascaded nanophotonic devices, since current study of nanophotonic devices mostly focuses on single device. Here, on-chip cascaded nanophotonic devices are designed based on an intelligent algorithm by combining genetic algorithm, simulated annealing algorithm and finite element method for the first time, and verified experimentally by using silicon-based planar structures. The cascaded devices consist of a bandpass filter and a wavelength router operating in optical communication range. The operation bandwidth of the bandpass filter is 408 nm with transmission more than 80%, within which the communication wavelengths of 1,300 nm and 1,550 nm are routed into different output ports through the wavelength router component. The footprint is only 3.62 μm^2 for the bandpass filter and only 2.56 μm^2 for the wavelength router, which are easy for integration with planar structures and ultrasmall size. This work provides a highly-efficient scheme for the realization of on-chip cascaded nanophotonic devices on the same chip, and lays a foundation for the realization of photonic chip based on intelligent algorithm.**

***Index Terms*—Bandpass filter, wavelength router, genetic algorithm, on-chip integration.**

Manuscript received May 28, 2021; revised July 9, 2021; accepted July 22, 2021. Date of publication July 27, 2021; date of current version August 24, 2021. This work was supported in part by the National Natural Science Foundation of China under Grants 91850117, 11604378, 11654003, 61775003, 11734001, 91950204, and 61775244, in part by Beijing Institute of Technology Research Fund Program for Young Scholars, National Key Research and Development Program of China under Grant 2018YFB2200403, and in part by Beijing Municipal Science & Technology Commission under Grant Z191100007219001. *(Hongyi Yuan and Lifeng Ma contributed equally to this work). (Corresponding authors: Cuicui Lu; Shuai Feng.)*

Hongyi Yuan, Lifeng Ma, and Jing Li are with the Beijing Key Laboratory of Nanophotonics and Ultrafine Optoelectronic Systems, School of Physics, Beijing Institute of Technology, Beijing 100081, China (e-mail: 2584557325@qq.com; 529389330@qq.com; 785514601@qq.com).

Zhe Yuan and Shuai Feng are with the School of Science, Minzu University of China, Beijing 100081, China (e-mail: yuanzhe1124@foxmail.com; fengshuai75@163.com).

Xiaoyong Hu is with the State Key Laboratory for Mesoscopic Physics & Department of Physics, Collaborative Innovation Center of Quantum Matter, Beijing Academy of Quantum Information Sciences, Nano-optoelectronics Frontier Center of Ministry of Education, Peking University, Beijing 100871, China (e-mail: xiaoyonghu@pku.edu.cn).

Cuicui Lu is with the Beijing Key Laboratory of Nanophotonics and Ultrafine Optoelectronic Systems, School of Physics, Beijing Institute of Technology, Beijing 100081, China, and also with the Collaborative Innovation Center of Light Manipulations and Applications, Shandong Normal University, Jinan 250358, China (e-mail: cuicuilu@bit.edu.cn).

Digital Object Identifier 10.1109/JPHOT.2021.3100357

I. Introduction

INTEGRATED nanophotonic devices are widely used in all-optical connection, all-optical computing, and all-optical network [1]–[3], etc. Nanoscale photonic devices are essential components for chip integration. They have great application potential in many research and technical fields such as high-performance computer, optical communication, quantum information and artificial intelligence, due to the broad bandwidth and large information capacity. There are various works [4]–[12] reported in recent years, but all of them are single devices with different realization schemes and different structure types or even different materials. No effective method has been found to design On-chip cascaded bandpass filter and wavelength router directly, which seriously restricts the development of integration for two or more nanophotonic devices. While cascading is an unavoidable step for integration, it is urgent to develop an efficient method for design of on-chip cascaded nanophotonic devices [13].

As for the cascaded nanophotonic devices, bandpass filters, as a fore-end signal processing device, are widely used [4], [14], in which light of unwanted band has a large attenuation while expected band can be obtained. At present, the bandpass filter can be designed based on bilayer fish-scale metamaterials [5], and it has a flat pass band but suffers from the shortcoming of big footprint, which is inconvenient for integration. Bandpass filter based on distributed Bragg reflector grating is smaller and the edges of passband are steep [15], but the bandwidth is limited. Besides the fore-end device, in the practical application of nanophotonic chip, devices are required to transmit different information into different channels, in which wavelength router is an essential component. Wavelength routers based on photonic crystal [10] and grating [11] have broad operation band but large size, which restricts the improvement of integration density when cascading with other nanophotonic devices. Surface plasmon polariton can be applied to design smaller wavelength router, however, it suffers from loss [8], [16]. There is a report about Mach-Zehnder wavelength filters [9], and it has the advantage of low insertion loss, but its size is still large due to the long arms on mm-level. Using micro-ring modulators to design wavelength division multiplexer leads to a smaller length ($\sim$10 μm) and has sharp peaks [17], however, the resonant wavelength of each micro-ring is sensitive to the radii thus deviation of nano-scale results in a noticeable difference, which is inconvenient for current fabrication technology. To sum up, traditional design methods are difficult to realize following

requirements simultaneously: ultrasmall size, broad bandwidth, fabrication convenience. To date, few reports have been found to provide efficient method for realizing high-performance on-chip cascaded bandpass filter and wavelength router. Although there is cascaded Mach-Zehnder wavelength filters for WDM (de-)multiplexing [18], the footprint of the cascaded devices is large, 500 $\times$ 400 μm^2, and intelligent algorithm is not applied on it. There is also cascaded system of metasurfaces designed by adjoint gradient method [19], but the system has a bulky volume compared with on-chip integrated cascaded devices. The lack of on-chip cascaded devices limits the development of integration for nanophotonic components.

In this work, we implement on-chip cascaded bandpass filter and wavelength router around the communication range based on an intelligent algorithm (IA) by combining genetic algorithm (GA), simulated annealing algorithm (SAA) and finite element method (FEM) for the first time. By combining GA with SAA, the intelligent algorithm will have bigger possibility to get out of local optimum, which will be explained in detail in the next part. The transmittance of the cascaded system is 85% at 1300 nm and 82% at 1550 nm. Two devices are cascaded together on the same chip to form an integrated nanophotonic system. By cascading the bandpass filter in front of the wavelength router, the system can route light of target wavelength bands distinctly while keeping the noise from unwanted band very low. In the experiment, on-chip nanophotonic devices are fabricated and measured successfully, which verifies the calculated results in the communication range. The footprint of the bandpass filter is only 3.62 μm^2 and the footprint of the wavelength router is only 2.56 μm^2.

II. Method

The cascaded bandpass filter and wavelength router are designed based on the IA, which consists of GA, SAA and FEM. As a general algorithm imitating natural evolution, GA regards design variable sequence as gene which is usually represented by binary code, and generates children with better performance by crossover and mutation [20]. GA is broadly used in optimization of complex questions. However, standard GA is easy to get stuck in local optimum because it selects parents for next generation according to fitness value: individuals with better fitness value have higher probability to be chosen and individuals with poorer fitness value but with good gene have little probability to be selected [21]. To get rid of this shortcoming, SAA is employed in selecting parents for next generation. SAA stimulates the gradual cooling process of solid, during which the particles within it come from disorder to order [22]. The way of SAA accepting new solution is Metropolis criterion which is based on current temperature [23]. According to Metropolis criterion, there is probability for solutions with poor performance to be accepted, which is beneficial for the algorithm to get out of local optimum. So, the introduction of SAA into GA makes it more possible for individuals with poorer fitness value but with good gene to be selected as parents than before. The probability of accepting an individual with poorer fitness value is shown below,

$$\mathrm{P} = \exp\left(\frac{\mathrm{f_{new}} - \mathrm{f_{old}}}{\mathrm{T}}\right), \ (\mathrm{f_{new}} < \mathrm{f_{old}}) \tag{1}$$

in which P is probability, $\mathrm{f_{new}}$ is the fitness value of the new child generated, $\mathrm{f_{old}}$ is the fitness value of the parent, and T is the temperature. The temperature T is set to decrease gradually during the optimization, which means the probability to accept poorer individuals will decrease as the iteration number increases, so the introduction of SAA will not weaken the convergence ability of GA.

Before the beginning of optimization, there are some conditions needed for a device, including shape, size, material and number of geometry unit. First, the shape and size of a device should be given. For the convenience of region's mathematical expression and fabrication, convex polygon is recommended. Second, the material of device decides the light control ability of the device. Considering current experiment conditions, silicon is selected as the base material. Finally, the device area is divided into a number of little areas by a set of orthogonal equidistant grids. Each little area corresponds to an air hole. In the evolution process, each air hole can only change its position and size within its divided area. By setting the density of grid, the number of air holes can be determined. When considering cascaded system, the presetting process is similar. The region of each part of the system can be expressed mathematically, and then each part is divided into little areas with its own grids. During the evolution process, the GA considers all little air holes at the same time. In the optimization process, all of the variables are regarded as set of genes, which means if genes are given, the corresponding structure is determined. In each generation, GA selects parents for next generation according to Metropolis criterion, and then GA use crossover among parents to inherit beneficial genes and use mutation to search better genes. Because of the employment of SAA, it is possible for GA to get the global optimum under pre-set conditions. GA's evolution direction is determined by fitness function, which is a function used to measure an individual's performance. Fitness function F can be expressed in a general form as below:

$$\mathrm{F} = \sqrt{\frac{1}{\mathrm{m}}\sum\nolimits_{i=1}^{m} {S_i}^2} - \frac{n}{\sum_{j=1}^{n} \frac{1}{T_j}}, \tag{2}$$

where S_i represents signal to be increased and T_j represents noise to be decreased. The evolution direction of GA is to get a better fitness value. In the design of device, select a suitable fitness function to describe the design target is vital. In this paper's design, the transmission spectrum of device is applied to construct fitness function. For those wanted wavelengths, square mean is applied on them, while harmonic mean is applied on other unwanted wavelengths. The stop condition for GA is that the average fitness value of group has no improvement in given number of iterations or the iteration number exceeds maximum. In each iteration of the optimization, the transmission spectrum is calculated through FEM which solves Maxwell's equations under given conditions.

III. Design and Analysis

A. Bandpass Filter

To begin with, the design of bandpass filter is taken as an example to illustrate the process of the intelligent algorithm (IA) by combining GA, SAA and FEM. First, the initial structure is pre-set. The shape of the device is an octagon with a footprint of 3.62 μm^2, whose side lengths are 1 μm except upper and lower sides of 500 nm. The port width of the device is set as 650 nm and the material of the octagon is pre-set, which can be any optical material with larger refractive index than air, here we use silicon-on-insulator (SOI). Second, GA randomly generates a given number of small geometries filled with air on the base of dielectric substrate. Third, IA calls FEM to calculate the performance of each individual device and then sends the value back to GA. After repeating the generating and evaluating process for a certain number of individuals, GA gets the first generation of the whole group. According to the fitness value and Metropolis criterion, GA selects parents to generate next generation. Iteration will not stop until the average fitness value of the group has no increase in the nearest several generations. Finally, the target bandpass filter is obtained. The fitness function is defined as the root-mean-square of signal, subtracting the harmonic mean of noise:

$$\text{fitness} = \sqrt{\frac{1}{m}\sum_{i=1}^{m} y(\lambda_i)^2} - n \times \left[\frac{1}{S} + \sum_{j=1}^{n} \frac{1}{y(\lambda_j)}\right]^{-1} \tag{3}$$

$$S = y_{pmax} - y_{pmin} \tag{4}$$

where y is the transmittance of different wavelength, while λ_i and λ_i (i, j = 1, 2, 3…) are the selected wavelength in the passband and the filtered band, respectively. In the second term, S is introduced to make the pass band flat. In the definition of S, y_{pmax} means the maximum of transmittance in the pass band while y_{pmin} is the minimum. By including the range of transmission of pass band into noise, the pass band of bandpass filter can be as flat as possible.

As mentioned above, in the optimization process of IA, thousands of individuals are calculated for evolution, so it is necessary to shorten the time of simulation. For this purpose, mode analysis module of physical field simulation software is used to calculate the effective refractive index, which can convert the 3D model into an equivalent 2D model [24]. The equivalent index method regards the three layers of material as the main factor and ignores the effect of internal pore structure, which is accurate enough in the allowed error range [25]–[27]. Take 1425 nm (the middle wavelength between 1300 nm and 1550 nm) as example, the calculated effective refractive index of the TE mode is 2.83, which is shown in Fig. 1(a). The thickness of air is 2000 nm, which is larger than an effective wavelength and is enough to simulate the real situation. And the Si slab is 220 nm thick. Under the Si slab, SiO_2 is 2000 nm thick. Furthermore, effective refractive indexes of Si at different wavelengths are studied to be used in the calculation, which is shown in Fig. 1(b).

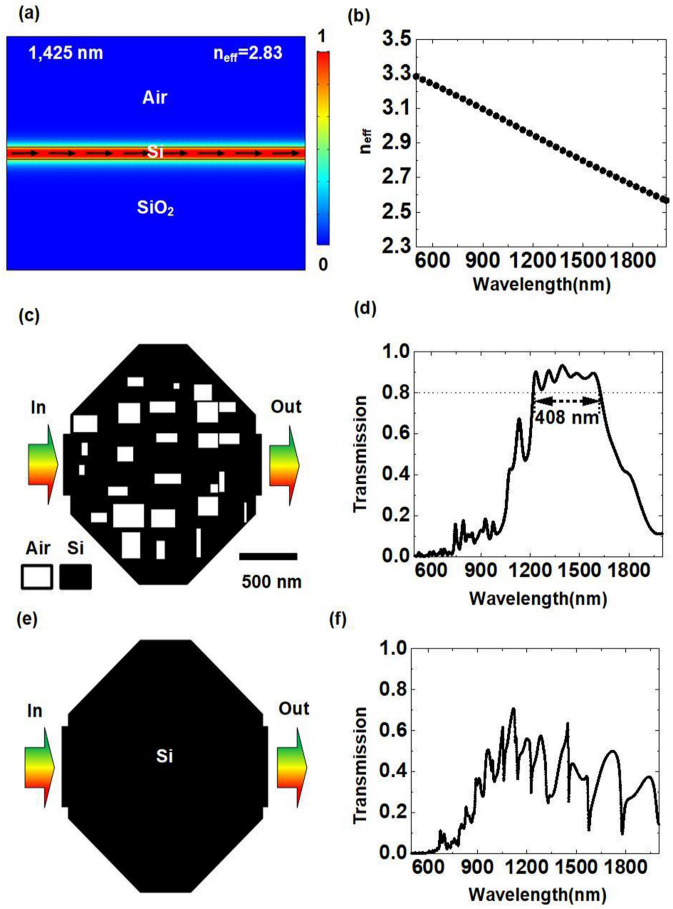

Fig. 1. (a) Effective refractive index of Si at 1425 nm for TE mode. The color represents the electric field distribution and black arrows represent the electric field direction. (b) The effective refractive index at different wavelength. (c) Structure of the bandpass filter. (d) The transmission spectrum of the bandpass filter. (e) A pure dielectric waveguide structure without air holes with the shape of the bandpass filter. (f) The transmission spectrum corresponding to the structure on the left side.

Considering the practical nano-fabrication, rectangle structure is chosen as the shape of the unit of small geometry. There is no limit of minimum side length of rectangle in order to get the best performance in the all parameter space. To evaluate the performance of the bandpass filter, TE-polarized light ranging from 500 nm to 2000 nm is introduced into the device from the left port, and FEM calculates the transmission spectrum at the right port, which is shown in Fig. 1(c). The final transmission spectrum is shown in Fig. 1(d). The bandwidth of the bandpass filter above 80% is 408 nm, from 1217 nm to 1625 nm, covering the wavelength band centers of 1300 nm and 1550 nm. The transmittance in the pass band (1220 nm to 1570 nm) is around 90%. The transmittance of 1300 nm and 1550 nm are 89% and 86%, respectively. Meanwhile, the average transmittances from 500 nm to 1000 nm and from 1900 nm to 2000 nm are pressed down to be lower than 10%. The footprint of the bandpass filter is only 3.62 μm^2. Moreover, an octagonal Si slab waveguide with exactly the same geometry parameters but without air holes is calculated to demonstrate the bandpass filter's modulation of

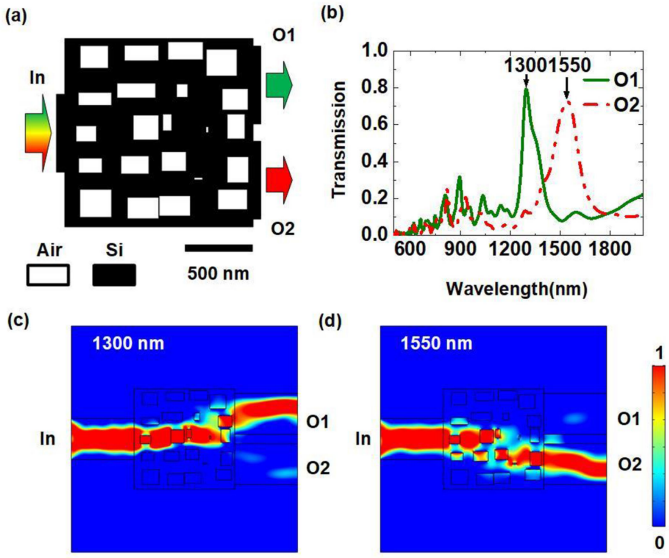

Fig. 2. Calculated results of the wavelength router. (a) The structure of the wavelength router. (b) The simulated transmission spectrum of the wavelength router. (c) and (d) The simulated electromagnetic energy density distribution of the wavelength router at 1300 nm and 1550 nm, respectively.

light. The structure is shown in Fig. 1(e). The corresponding transmission spectrum is shown in Fig. 1(f). It can be seen that without air holes, the spectrum is irregular and with a high loss caused by the dielectric waveguide mode and resonant modes within the waveguide sides. If there is no internal structure, the light will suffer from great loss during the propagation.

B. Wavelength Router

In this section, a wavelength router working in the communication band is designed in the communication band. As shown in Fig. 2(a), the shape of the wavelength router is set as a square with side length of 1.6 μm, corresponding to a footprint of 2.56 μm^2. Considering the integration applications, we use the same material of SOI with the above bandpass filter. The units of small geometry are set as rectangles for the convenience of fabrication. The rectangles have no limit of minimum side length in order to seek the best performance in simulation. The width of the three ports is set as 650 nm and TE-polarized light is input at the left port and detected at the right ports. The band of input light is set from 1000 nm to 1850 nm, and light around 1300 nm outputs mainly at the upper right port, O1, while light around 1550 nm outputs at the lower right port, O2.

In the process of designing the wavelength router by IA, the fitness value of the wavelength router is set as followed:

$$\text{Fitness} = \sqrt{\frac{1}{2}\left[\text{y}(\lambda_{1300})^2 + \text{y}(\lambda_{1550})^2\right]} - \text{n} \times \left[\sum_{\text{j}=1}^{\text{n}} \frac{1}{\text{y}\,(\lambda_{\text{j}})}\right]^{-1} \quad (5)$$

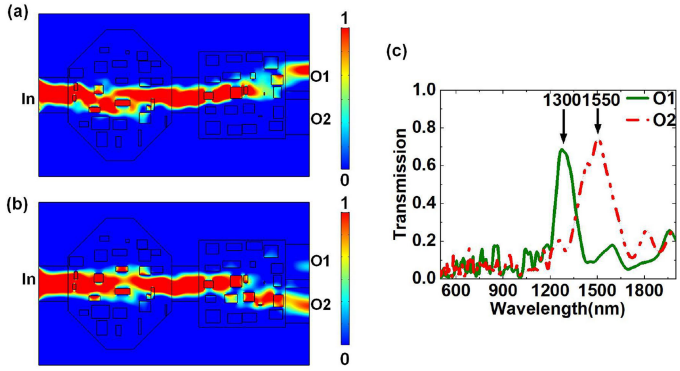

Fig. 3. Calculated results of cascaded devices. The electro-magnetic energy distribution of 1300 nm (a) and 1550 nm (b), respectively. (c) The transmission spectrum of cascaded devices.

where y is the transmittance of different wavelength, and λ_{1300} and λ_{1550} represent the wavelength of 1300 nm and 1550 nm respectively. The wavelength of noise points is represented by λ_i.

After the similar iteration processes described above, the final structure is generated and presented in Fig. 1(a). The corresponding transmission spectrum is shown in Fig. 2(b). The wavelength router divides light with 1300 nm and 1550 nm distinctly. The transmittance of 1300 nm is 78% while that of 1550 nm is 72%. This is better than what we have done before [25] using the intelligent algorithm which only combines GA and FEM. The electromagnetic energy density distributions of 1300 nm and 1550 nm are plotted in Fig. 2(c) and Fig. 2(d), respectively. It can be seen distinctly that the light of 1300 nm propagates to the upper right port while the light of 1550 nm propagates to the lower right port.

C. Cascading and Analysis

Finally, two devices are cascaded together on the same chip to study the transmission spectrum. TE-polarized light ranging from 500 nm to 2000 nm is introduced into the system via a waveguide. The bandpass filter and the wavelength router are connected with a waveguide of 500 nm in length. Waveguides have the same width of 650 nm in order to support the same modes. The simulated result is shown in Fig. 3. The electromagnetic energy distribution is shown in Fig. 3(a) and (b). Light of 1300 nm and 1550 nm output from the output ports O1 and O2 on the right side, respectively. The transmission spectrum is shown in Fig. 3(c).

By comparing with the transmission of wavelength router, it is shown that the noise away from 1300 nm and 1550 nm is filtered by the former bandpass filter. The average transmittance of noise from 800 nm to 1100 nm is suppressed below 5.2% of cascaded device, which is 13.5% in the wavelength router. The peak transmittance of 1300 nm and 1550 nm are 52.6% and 62.3%, respectively. By cascading the bandpass filter before the wavelength router, the system can achieve a function that expected band can be selected from a broad range of wavelength (500 nm $\sim$ 2000 nm) while noise coming from high frequency

TABLE 1
COMPARISON OF REPORTED WORKS OF DESIGNING NANOPHOTONIC DEVICES USING ALGORITHM SINCE 2015

Year	2015	2016	2017	2018	2019	2020	2021
References	Shen et al. [28]	Frellsen et al. [29]	Piggott et al. [30]	Chang et al. [31]	Vercruysse et al. [32]	Cuicui Lu et al. [33]	This work
Method	Direct-binary search	Topology optimi-zation	Inverse design algorithm	Direct-binary search	Inverse design with analytical level set fabrication constraints	Genetic algorithm, finite element method	GA, SAA, FEM
Calculation Time	~140 hours (hardware conditions unknown)	~8 hours (on 112 CPUs with XeonE5-266 5 cores connected with infiniband)	~2 hours (on a single server with an Intel Core i7-5820K processor, 64 GB of RAM, and three Nvidia Titan Z graphics cards)	~28 hours (on a computer with an 8-core central processing unit of Intel Xeon E5-2637)	--	~2 hours (on a personal computer with 4 Intel Core i7-7500U CPU, and 8 GB of RAM)	~6 hours (on a personal computer with 4 Intel Core i7-7500U CPU, and 12G of RAM)
Iteration Number	~400	~200	~18	–	~150	~200	~200
Designed Devices	Polarization beam-splitter	Mode demulti-plexer	Power splitter	Dual- mode 3 dB power splitter	Waveguide demulti-plexer	Polari-zation router	Cascaded bandpass filter and wavelength router
Device Footprint	2.40 × 2.40 μm^2	2.60 × 4.22 μm^2	3.80 × 2.50 μm^2	2.88 × 2.88 μm^2	2.50 × 2.50 μm^2	0.97 × 1.24 μm^2	4.01 × 2.41 μm^2

band is filtered. These cascaded devices can be achieved because the same design framework is applied to two different devices, which promises parameters, like slab thickness and work band, to be the same. Effective refractive index method is also used in simulation. The time cost of the whole design is about 6 hours, after 200 iterations of optimization, using 4 Intel (R) Core (TM) i7-7500U CPU at 2.7 GHz, and 12G installed memory (RAM, random access memory).

Furthermore, we make a table to compare our work with several reported works in nanophotonic device design using algorithm. There are many good works in recent years, we just select one typical work in related field for each year. It can be seen that reports before are concentrated on single device design and there is a lack of report about on-chip cascaded nanophotonic devices.

The function of the designed structures can be understood physically from the photonic Anderson localization theory [25], [34], [35]. In the disordered structure designed by IA, each inner rectangular structure can be considered as an optical scatter, which produces multiple scattered optical waves [36], [37]. When the multiple scattered waves interfere with each other, they form a variety of localized modes and guided modes in the disordered structures. The localized modes are generally trapped in the structure, while the guided modes can form microchannels for light transmission. In the bandpass filter structure, the wavelengths of incident light that match the guided modes can transmit through the structure, which forms passband with high transmission. Meanwhile, the incident wavelengths that do not match the guided modes will be forbidden. Therefore, different incident wavelengths and structures corresponding to different transmission, and devices with different functions can be designed. Based on the same principle, cascaded bandpass filter and wavelength router can also be designed successfully by our IA, and the fitness function is also expressed by the difference between signal and noise mentioned above. The final structure parameters are given after iterations of about two hundred times by IA, where multiple localized modes and guided modes can be formed to meet the target function in our algorithm.

IV. EXPERIMENTAL RESULTS

To verify the performance of the bandpass filter, wavelength router and cascaded devices, the devices are fabricated and measured experimentally. Considering the real fabrication process, the smallest size of side length for the unit cell is forced to be larger than 50 nm in the device structure, and we design various samples. At the same time, we use disordered gratings as the

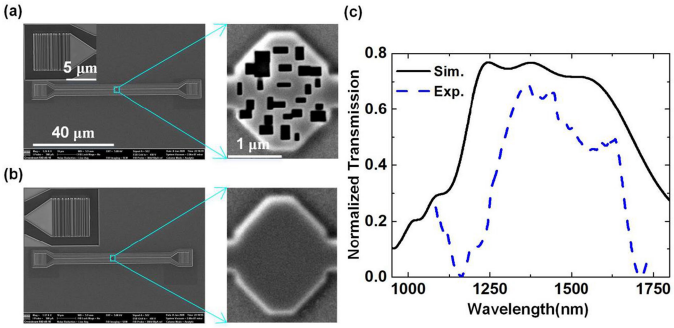

Fig. 4. The SEM images of the sample (a) and reference sample (b) of the bandpass filter. The left is the whole image of sample, the upper left corner is the grating, and the right is an enlarged view of the central structure of the sample and reference sample. (c) Experimental and simulated normalized transmission spectra.

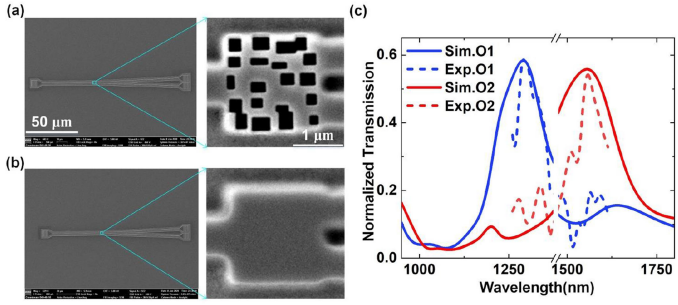

Fig. 5. The SEM images of the sample (a) and reference sample (b) of the wavelength router. The left is the whole image of sample, and the right is an enlarged view of the central structure of the sample and reference sample. (c) Experimentally measured (Exp.O1, Exp.O2) and simulated (Sim.O1, Sim.O2) transmission spectra. The central wavelength of the output port of the wavelength router are 1300 nm and 1550 nm respectively, and the corresponding transmittance of both the measured and simulated central wavelength is 58% and 54% respectively. Since the range of the laser is 130 nm in one test, and considering the different functions realized by the devices, the continuous spectrum of the bandpass filter is measured, while the wavelength router is measured the band near the center wavelength. A break point of 120 nm is set in the middle of the band, which does not affect the test of transmittance at the central wavelength.

excitation ports to improve the conversion efficiency, which are optimized by the IA, too [33].

The entire sample fabrication process is performed on a SOI plate, and etched using the scanning electron microscopy (SEM)/focused ion beam (FIB) system (ZEISS Crossbeam 540). The samples of bandpass filter, wavelength router and their cascaded devices are measured by optical microspectral measurement system. In the process of measurement, a supercontinuum wave (SCW) laser (YSL SC-5) is used to provide signal light excitation, and a spectrometer (Andor 303i) is used to measure the distribution of wavelength at each port. The etched parts include the coupling ports and waveguides of the samples and reference samples, and the rectangular holes of the central structure of the samples. The voltage of the whole etching process is fixed at 30 kV. The etching ion beam of the coupling ports and waveguides are 50 pA and 300 pA, respectively. The beam of 5 pA is used to etch the internal structure. In addition, since the detection range of the spectrometer is limited to the near-infrared band, it can only make measurement in the range of 130 nm at one time, so the complete transmittance cannot be determined at one time. Therefore, we adopt the method of multiple measurements to measure the transmission spectrum of the bandpass filter structure and cascaded devices in the form of segments, and finally obtain the experimental results. The following are the specific test steps: first, locate the etched sample and the reference sample under an optical microscope. Next, adjust the polarizer, and measure the background field. Then, turn on the laser, set the corresponding center wavelength in the spectrometer software, and determine the measured spectrum. Go through the above steps, the samples and their corresponding reference samples will be measured one by one.

At the end of the waveguide, disordered gratings are etched to form a grating that coupling light from free space to an on-chip waveguide, so that the signal can be detected more effectively. However, the traditional grating coupler has a large volume. Therefore, we also use the IA to design the disordered coupling ports [33]. The footprint of the coupling ports is 36 μm^2, the length and the width are both 6 μm, the central structure is a rectangular grating, and the depth of the rectangular grating is 110 nm. The SEM images of the grating are shown in the upper left corner of A and B in Fig. 4. The maximum excitation efficiency of coupling port can reach 13.75%. The length of the waveguide is 30 μm and the width keeps 650 nm.

The SEM images of etched samples and reference samples of bandpass filter are shown in Fig. 4(a) and Fig. 4(b), respectively. The figure on the left is the whole fabricated structure, the right part is an enlarged view of the internal structure, and the black part is the etched rectangular hole in the central structure. Fig. 4(c) is the normalized transmission spectrum of experimental and theoretical simulation. In the simulation, the power of incident light is set to 1. In this way, when the light travels along the designed optical path, the power measured at the probe location after passing through the device is the normalized transmittance of the device. In the experiment, in order to minimize the effects of background noise, a blank control group composed of devices with no internal structure is set. Because input light is set the same in two measurement, the normalized transmission can be evaluated by comparing the etched structure to blank structure. When the incident light with the same intensity is coupled to the optical path, the ratio of the transmittance measured at the port of the designed device to that measured at the port of the blank control group is the normalized transmittance. To eliminate the influence of coupling efficiency, sensitivity of grating and light source on the experimental results of different wavelengths, the normalized transmission shown in the figure is the ratio of the transmittance of the sample port to that of the reference sample port [25], [33]. It can be seen that the bandwidth of the bandpass filter is a little bit narrower than that in the theoretical calculation. This is mainly due to some unavoidable fabrication errors in the experiment. Because the FIB etching process is not perfect, certain material deposition will occur on the inner wall of the etched structure. The corner of the rectangular hole is not square, but like a round corner. In the optimization of the internal structure of the experimental sample, the internal rectangular hole length is set to be no less than

50 nm to meet the requirement of machining accuracy, that is, the structure of experimental sample is a little bit different from the optimal structure obtained in the simulation, which leads to the transmittance of the experimental sample is slightly lower. Therefore, the bandwidth can be enlarged and the signal strength can be improved by improving the manufacturing process and removing noise. In spite of this, the transmittance of the passband is high, and the transmittance outside the passband drops sharply, which indicates that the structure achieves the band pass function in the near-infrared band.

In addition, the fabrication error tolerance is calculated. The fabrication error tolerance is defined as the maximum displacement that each structural element can move. For each internal structural element, the positions of all holes are randomly moved within a certain distance, and then the corresponding transmission spectrum is calculated. Unified fault-tolerant standards are established in terms of the allowable offset of the central wavelength, the relative reduction of the maximum transmission and the absolute increment of the maximum noise of each wavelength. The calculation results show that the average position error of the designed cascaded devices is about 30 nm, which fully meets the current nanomanufacturing technology, and this error range is also acceptable [33].

The fabrication and measured results of the wavelength router are shown in Fig. 5. The left side of Fig. 5(a) and (b) are the whole image of the sample and the reference sample, respectively. The core structure of the sample is shown on the right side of Fig. 5(a) and the reference sample is shown on the right side of Fig. 5(b), with a footprint of 2.56 μm^2. The normalized transmittance spectra of experimental and theoretical simulation are shown in the Fig. 5(c). The theoretically simulated transmittance of the wavelength router is 58% and 54% respectively, and the measured normalized transmittance of the upper and lower ports on the right is 58% and 54% respectively, too. The experimental results demonstrate that the two communication bands with center wavelengths of 1300 nm and the 1550 nm are successfully routed into different channels.

The fabrication and measured results of cascaded devices of wavelength router and bandpass filter are shown in Fig. 6. On the left side of Fig. 6(a) and (b) are the whole image of the cascaded devices, the sample and the reference sample, respectively. Their corresponding central structures are on the right side of Fig. 6(a) and (b). First the light in the waveguide passes through the bandpass filter, and then it passes through the wavelength router, and finally comes out from the two ports. The transmittances of the upper right and lower right ports in the experiment and calculation are shown in Fig. 6(c), respectively, which indicates that the cascaded devices based on IA has provided an effective method for the realization of on-chip cascaded nanophotonic devices.

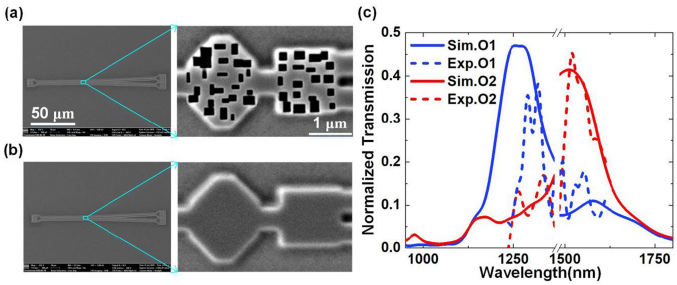

Fig. 6. The SEM images of the sample (a) and reference sample (b) of the cascaded devices. The left is the whole image of sample, and the right is an enlarged view of the central structure of the sample and reference sample. The length of the waveguide between the cascaded is 500 nm. (c) Experimentally measured (Exp.O1, Exp.O2) and simulated (Sim.O1, Sim.O2) transmission spectra. Since the range of the laser is 130 nm in one test, a break point of 120 nm is set in the middle of the band, which does not affect the test of transmittance at the central wavelength.

V. Conclusion

In conclusion, on-chip cascaded nanophotonic devices are designed based on a constructed intelligent algorithm and verified experimentally. By employing IA, on-chip cascaded devices consist of a bandpass filter and a wavelength router is designed and fabricated. The length of the whole cascaded system is within 3.6 μm, which is the smallest one in reported works. The footprint of the bandpass filter and the wavelength router are 3.62 μm^2 and 2.56 μm^2 accordingly. The bandwidth of the bandpass filter is 408 nm with transmission more than 80%. The wavelength router divides 1300 nm and 1550 nm distinctly. This work provides a highly effective scheme for the realization of on-chip cascaded nanophotonic devices, and may bring more opportunities for the realization of multifunctional nanophotonic devices.

References

[1] C. Sun *et al.*, "Single-chip microprocessor that communicates directly using light," *Nature*, vol. 528, no. 7583, pp. 534–583, 2015.
[2] P. Kok, W. J. Munro, K. Nemoto, T. C. Ralph, J. P. Dowling, and G. J. Milburn, "Linear optical quantum computing with photonic qubits," *Rev. Mod. Phys.*, vol. 79, no. 1, pp. 135–174, 2007.
[3] E. D. D. J. Manley, "All-optical network coding," *J. Opt. Commun. Netw.*, vol. 2, no. 4, pp. 175–191, 2010.
[4] D. Gerz *et al.*, "Mid-infrared long-pass filter for high-power applications based on grating diffraction," *Opt. Lett.*, vol. 44, no. 12, pp. 3014–3017, 2019.
[5] X. Zhang, J. Gu, W. Cao, J. Han, A. Lakhtakia, and W. Zhang, "Bilayer-fish-scale ultrabroad terahertz bandpass filter," *Opt. Lett.*, vol. 37, no. 5, pp. 906–908, 2012.
[6] J. Han, J. Gu, X. Lu, M. He, Q. Xing, and W. Zhang, "Broadband resonant terahertz transmission in a composite metal-dielectric structure," *Opt. Exp.*, vol. 17, no. 19, pp. 16527–16534, 2009.
[7] Y. Chiang, C. Yang, Y. Yang, C. Pan, and T. Yen, "An ultrabroad terahertz bandpass filter based on multiple-resonance excitation of a composite metamaterial," *Appl. Phys. Lett.*, vol. 99, no. 19, 2011, Art. no. 191909.
[8] X. Huang *et al.*, "All-Dielectric metasurfaces color filter arrays designed by evolutionary search," *IEEE Photon. J.*, vol. 13, no. 3, Jun. 2021, Art. no. 7100409.
[9] F. Horst, W. Green, S. Assefa, S. Shank, Y. Vlasov, and B. Offrein, "Cascaded Mach-Zehnder wavelength filters in silicon photonics for low loss and flat pass-band WDM (de-)multiplexing," *Opt. Exp.*, vol. 21, no. 10, pp. 11652–11658, 2013.
[10] M. Nawwar, H. Shalaby, and R. K. Pokharel, "Photonic crystal-based compact hybrid WDM/MDM (de) multiplexer for SOI platforms," *Opt. Lett.*, vol. 43, no. 17, pp. 4176–4179, 2018.
[11] N. A. Idris *et al.*, "Full-mesh T- and O-band wavelength router based on arrayed waveguide gratings," *Opt. Exp.*, vol. 24, no. 1, pp. 672–686, 2016.

[12] D. Dai, Z. Wang, J. Peters, and J. E. Bowers, "Compact polarization beam splitter using an asymmetrical Mach–Zehnder interferometer based on silicon-on insulator waveguides," *IEEE Photon. Technol. Lett.*, vol. 24, no. 8, pp. 673–675, Apr. 2012.
[13] A. S. Backer, "Computational inverse design for cascaded systems of metasurface optics," *Opt. Exp.*, vol. 27, no. 21, pp. 30308–30331, 2019.
[14] P. Li *et al.*, "Observation of flat chaos generation using an optical feedback multi-mode laser with a band-pass filter," *Opt. Exp.*, vol. 27, no. 13, pp. 17859–17867, 2019.
[15] P. Sah, and B. K. Das, "Integrated optical rectangular-edge filter devices in SOI," *J. Lightw. Technol.*, vol. 35, no. 2, pp. 128–135, 2017.
[16] C. Lu, Y. Liu, X. Hu, H. Yang, and Q. Gong, "Integrated ultracompact and broadband wavelength demultiplexer based on multi-component nano-cavities," *Sci. Rep.*, vol. 6, 2016, Art. no. 27428.
[17] Q. Xu, B. Schmidt, J. Shakya, and M. Lipson, "Cascaded silicon micro-ring modulators for WDM optical interconnection," *Opt. Exp.*, vol. 14, no. 20, pp. 9431–9436, 2006.
[18] F. Horst, W. M. J. Green, S. Assefa, S. M. Shank, Y. A. Vlasov, and B. J. Offrein, "Cascaded mach-zehnder wavelength filters in silicon photonics for low loss and flat pass-band WDM (de-)multiplexing," *Opt. Exp.*, vol. 21, no. 10, pp. 11652–11658, 2013.
[19] A. S. Backer, "Computational inverse design for cascaded systems of metasurface optics," *Opt. Exp.*, vol. 27, no. 21, pp. 30308–30331, 2019.
[20] D. Whitley, "A genetic algorithm tutorial," *Statist. Comput.*, vol. 4, no. 2, pp. 65–85, 1994.
[21] M. P. Hari, C. Ankit, and M. Deepti, "A comparative review of approaches to prevent premature convergence in gA," *Appl. Soft Comput.*, vol. 24, pp. 1047–1077, 2014.
[22] A. Corana, M. Marchesi, C. Martini, and S. Ridella, "Minimizing multimodal functions of continuous variables with the 'Simulated annealing' algorithm," *ACM Trans. Math. Softw.*, vol. 13, no. 3, pp. 262–280, 1987.
[23] N. Metropolis, A. W. Rosenbluth, and M. N. Rosenbluth, "Equation of state calculations by fast computing machines," *J. Chem. Phys.*, vol. 21, no. 6, pp. 1087–1092, 1953.
[24] V. Liu, D. A. B. Miller, and S. Fan, "Highly tailored computational electromagnetics methods for nanophotonic design and discovery," in *Proc. IEEE*, vol. 101, no. 2, pp. 484–493, 2013.
[25] Z. Liu *et al.*, "Integrated nanophotonic wavelength router based on an intelligent algorithm," *Optica*, vol. 6, no. 10, pp. 1367–1373, 2019.
[26] S. Dwivedi *et al.*, "Experimental extraction of effective refractive index and thermo-optic coefficients of Silicon-on-Insulator waveguides using interferometers," *J. Lightw. Technol.*, vol. 33, no. 21, pp. 4471–4477, 2015.
[27] N. Yokouchi, A. J. Danner, and K. D. Choquette, "Etching depth dependence of the effective refractive index in two-dimensional photonic-crystal-patterned vertical-cavity surface-emitting laser structures," *Appl. Phys. Lett.*, vol. 82, no. 9, pp. 1344–1346, 2003.
[28] B. Shen, P. Wang, R. Polson, and R. Menon, "An integrated-nanophotonics polarization beamsplitter with $2.4\times$ 2.4 μm 2 footprint," *Nat. Photon.*, vol. 9, no. 6, pp. 378–382, 2015.
[29] L. F. Frellsen, Y. Ding, O. Sigmund, and L. H. Frandsen, "Topology optimized mode multiplexing in silicon-on-insulator photonic wire waveguides," *Opt. Exp.*, vol. 24, no. 15, pp. 16866–16873, 2016.
[30] A. Y. Piggott, J. Petykiewicz, L. Su, and J. Vučković, "Fabrication-constrained nanophotonic inverse design," *Sci. Rep.*, vol. 7, no. 1, pp. 1–7, 2017.
[31] W. Chang *et al.*, "Inverse design and demonstration of an ultracompact broadband dual-mode 3 dB power splitter," *Opt. Exp.*, vol. 26, no. 18, pp. 24135–24144, 2018.
[32] D. Vercruysse, N. V. Sapra, L. Su, R. Trivedi, and J. Vučković, "Analytical level set fabrication constraints for inverse design," *Sci. Rep.*, vol. 9, no. 1, pp. 1–7, 2019.
[33] C. Lu *et al.*, "Nanophotonic polarization routers based on an intelligent algorithm," *Adv. Opt. Mater.*, vol. 8, no. 10, 2020, Art. no. 1902018.
[34] H. H. Sheinfux, Y. Lumer, G. Ankonina, A. Z. Genack, G. Bartal, and M. Segev, "Observation of anderson localization in disordered nanophotonic structures," *Science*, vol. 356, no. 6341, pp. 953–956, 2017.
[35] T. Schwartz, G. Bartal, S. Fishman, and M. Segev, "Transport and anderson localization in disordered two-dimensional photonic lattices," *Nature*, vol. 446, no. 7131, pp. 52–55, 2007.
[36] H. Cao *et al.*, "Spatial confinement of laser light in active random media," *Phys. Rev. Lett.*, vol. 84, no. 24, pp. 5584–5587, 2000.
[37] S. John, "Localization of light," *Phys. Today*, vol. 44, no. 5, pp. 32–40, 1991.